A novel approach for the closure of large damage in self-healing elastomers using magnetic particles

Cerdan Gomez, Kenneth; Van Assche, Guy; Van Puyvelde, Peter; Brancart, Joost

Published in:
Polymer

DOI:
10.1016/j.polymer.2020.122819

Publication date:
2020

License:
CC BY-NC-SA

Document Version:
Accepted author manuscript

A Novel Approach for the Closure of Large Damage in Self-Healing Elastomers Using Magnetic Particles

Kenneth Cerdan [1], Guy Van Assche [2], Peter van Puyvelde [1] and Joost Brancart [2]*

[1] Dept. of Chemical Engineering, Soft Matter, Rheology and Technology (SMaRT), KU Leuven, Celestijnenlaan 200F, 3001 Leuven, Belgium; kenneth.cerdangomez@kuleuven.be; peter.vanpuyvelde@kuleuven.be
[2] Physical Chemistry and Polymer Science (FYSC), VUB, Pleinlaan 2, B-2050 Brussels, Belgium; joost.brancart@vub.be; guy.van.assche@vub.be
* Correspondence: joost.brancart@vub.be

Abstract

Self-healing materials have been intensively studied as materials that can mimic healing properties of biological systems. Reversible polymeric networks based on Diels-Alder thermoreversible covalent bonds exhibit great healing performance by controlling the temperature of the system. Despite the attractive applications of self-healing materials, most of them are restricted to the repair of narrow cracks due to their restricted mobility in the solid state. In this work, magnetite (Fe_3O_4) particles are used to create self-healing magnetic composites. The use of a conventional magnet to apply a magnetic driving force is proposed for the closure of wide damage gaps in the solid state without the need of either mechanical intervention or liquid-like flow inside the material, limiting the structural stability. Thermal, mechanical and chemical characterization of different composites are performed in this study and the healing efficiency is evaluated to assess their potential to close and heal large damage sizes.

Keywords:
Magnetic composites · Self-healing polymer · Diels-Alder

1. Introduction

The continuous development of material science and technology has underpinned the basis of evolution of humankind. A better understanding of the intrinsic behaviour of materials gives rise to the possibility to modify their composition and physicochemical properties, tailoring their properties to our needs. An emerging example of smart, advanced materials is the class of stimuli-responsive materials, which can reversibly modify one or more of their properties under the application of an external trigger in a controlled fashion [1]. The activational trigger can be based on changes in temperature, pH, application of an external mechanical force, irradiation with light at a certain wavelength or by the presence of an external electrical or magnetic field [2]. These materials have showed interesting results in a wide range of different applications, including coatings [3,4], drug delivery [5,6], electronics [7,8] and actuators [9,10].

Inspired by nature, engineering new materials that can heal external damage, mimicking biological skin systems, is attainable with the development of the so-called self-healing (SH) materials. SH-materials are able to repair damage upon activation of a healing mechanism, often activated by changes in the environment surrounding the material. The ability to heal damage extends their lifetime, reliability and safety, and decreases the need for costly maintenance. Often, self-healing materials are classified as extrinsic or intrinsic SH materials, according to how the mechanism to repair damage is achieved in the material. For extrinsic SH materials, the healing ability is built-in, usually via encapsulation of healing agents inside microcapsules [11] or vascular networks [12]. In case of intrinsic materials, the healing functionality is inherent to the material system as a result of physicochemical interactions [13] or dynamic covalent chemical bonds [14].

Thermoreversible covalent bonds have received a great deal of attention during the past few decades, emphasizing those based on the formation of reversible Diels-Alder (DA)

crosslinks [4,15–17]. The DA reaction is a concerted $4\pi+2\pi$ cycloaddition of a conjugated diene and a dienophile employed for the formation of six-membered and polycyclic ring systems [18,19]. The $4\pi+2\pi$ cycloaddition takes place between furan and maleimide groups as a diene and dienophile, respectively. The reaction kinetics and thermodynamics are based on the shifting of the chemical equilibrium reaction towards the formation of the DA product (DA adduct) at low temperatures and promoting the reverse dissociation reaction at high temperatures, restoring the initial monomers (retro-DA reaction). The healing is either activated by mechanical breaking of the bonds or by increasing the temperature, shifting the equilibrium towards the breaking of the adducts, leading to the formation of free furan and maleimide groups. This increases the mobility in the material as a consequence of the decreased crosslink density, while retaining enough crosslinks points to preserve the solid state [20]. Because of the increase in the mobility of the material, the micro-macroscopic damage can be sealed, and upon cooling, the shift of the equilibrium is reversed, resulting in the reformation of the crosslinks in the network and, hence, the recovery of the initial properties. Controlling the DA crosslink density and polymeric chain length allows the manufacturing of a wide variety of distinct materials with different thermal and mechanical properties, ranging from stiff, hard thermosets [21,22] to elastic, soft elastomers [17,23].

All self-healing materials, extrinsic or intrinsic, need sufficient mobility to close the damage and to activate the healing process. To this end, an intimate contact between broken surfaces is necessary for intrinsic SH materials, while in extrinsic SH materials the healing agent can fill narrow cracks by way of capillary action. In most cases, this contact is only possible if damage dimensions are narrow, allowing the material with sufficient mobility to react across the broken surfaces (sharp cuts, scratches, perforations...). In the case of large damage, to the author's knowledge, the damage recovery is only possible in three different ways: (i) applying an external mechanical force, by way of human intervention, resulting in an lack of autonomy of the process, (ii) closing of the small gaps by way of elastic recovery of the material after the damaging force has been removed or the use of the shape-memory effect, designed into the material structure. This method, known as shape memory assisted self-healing (SMASH), is a nice approach but it is based on complex systems and microstructures, so it is highly dependent of complicated synthesis or elaborate fabrication processes [24,25], (iii) using a two-stage extrinsic SH approach where in a first stage a gelling agent is released to create a scaffold in the large damage volume, in which a healing agent can flow and cure to repair the damage in the second stage [26]. In this case, the healing cycles of extrinsic systems are limited, as the healing agent is consumed after the healing process. In this regard, it is desired to find new approaches for the closure of large damage in easily synthesizable and cost-affordable materials, so they are able to heal autonomously upholding their applicability.

This article presents a novel approach to heal large damage by dispersing magnetite (Fe_3O_4) within an elastomeric thermoreversible covalent network based on the DA chemistry. Magnetic nanoparticles of iron oxides have been intensively studied as a result of their technological applications, pointing out data storage [27], biosensors [28], drug delivery [29], wastewater treatment [30], materials science [31] and catalysis [32,33], among others. Incorporation of magnetic particles within self-healing materials has received research attention for different applications. Magnetic self-healing hydrogels have shown interesting results as potential injectable drug carriers with excellent biocompatibility [34,35]. An interesting approach is the use of magnetic particles to produce hysteresis heating under the application of an oscillating magnetic field, hence self-repairing cracks by promoting flow of the interfacial regions [36–38]. Other applications such as direct furan-functionalization of Fe_3O_4 nanoparticles as reversible crosslink centers [39] or the development of self-healing magnetic elastomers with shape memory effect [40] have been explored. The recovery of conductive properties and healing of external fractures through incorporation of permanent magnetic microparticles within conductive graphitic inks resulted in a potential candidate for long-lasting printed electronic devices [41].

Immobilization of magnetic nanostructures into a polymeric matrix leads to the formation of integrated functional systems which can interact with an external magnetic field. The

resulting magnetic force may be used to manipulate the motion or shape of the material in a controlled fashion. In this study, the effect of different filler loadings of the magnetic particles on the thermomechanical, viscoelastic properties and on the self-healing behaviour is assessed. By placing the broken material close to a permanent magnet, while heating the material, an enhancement of the viscous behaviour as a result of the temperature increase allows the material to have enough mobility to move along the magnetic field without the need to degel (transition from solid to liquid state in amorphous polymers), aligning broken surfaces and sealing the damage.

2. Materials and Methods

2.1. Materials

The chemicals employed for the synthesis of the materials are shown in Figure 1. The polyethertriamine Jeffamine T5000 with average degree of polymerization x+y+z (determined by NMR) of 85 ($\overline{M_n}$ = 5649 g/mol) was kindly provided by Huntsman Corporation. Furfuryl glycidyl ether (FGE, 96%), 1,1'-2(Methylenedi-1,4-phenylene)bismaleimide (DPBM, 95%) and Iron (II, III) oxide nanopowders (Fe_3O_4, 50-100 nm, BET surf. area 20-50 $m^2\ g^{-1}$, 4.8 - 5.1 g ml^{-1}, 97% trace metals basis) were obtained from Sigma Aldrich, and Hydroquinone was obtained from Chimica.

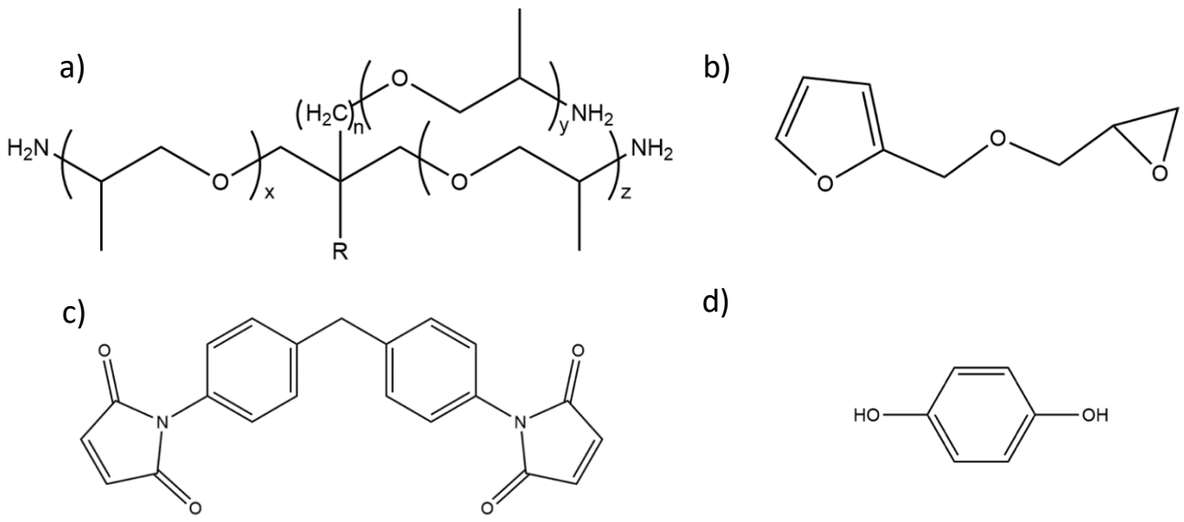

Figure 1. Chemical reactants employed for the synthesis of the Diels-Alder thermoreversible materials: a) Jeffamine T5000 (x + y + z = 85) b) Furfuryl Glycidyl Ether (FGE) c) 1,1'-(methylenedi-1,4-phenylene)bismaleimide (DPBM) d) Hydroquinone

2.2. Synthesis of the magnetic self-healable polymers

The synthesis of the magnetic materials was carried out using a 2-step synthesis procedure, by first performing the solventless epoxy-amine reaction between the Jeffamine T5000 and FGE at 90 ˚C until completion in a sealed container to generate the furan-functionalized monomer, named F5000. Subsequently, the monomers F5000 and DPBM were mixed in chloroform and magnetically stirred at room temperature until DPBM was completely dissolved. Hydroquinone was added as a radical inhibitor, to prevent side reactions such as the maleimide homopolymerization [42]. Once the monomers were completely dissolved, different loadings of Fe_3O_4 nanoparticles (NPs) were added to the solution, and mechanically shaken for one day to homogenize and properly disperse the particles in the solution. While shaking, the container was opened to let the chloroform evaporate and speed up the polymerization.

2.3. Characterization

2.3.1. Scanning Electron Microscopy (SEM)

The distribution and size of the Fe_3O_4 particles was visualized by using a JEOL JSM-6010LV SEM, operating at 10 kV accelerating voltage. All samples were sputter coated with a thin

Au/Pd layer by a JEOL JFC-1300 autofine coater in order to minimize sample charging during imaging.

2.3.2. FTIR Spectroscopy

The Diels-Alder reaction was studied using a Thermo Fisher Scientific Nicolet 6700 FT-IR spectrometer. An attenuated total reflectance (ATR) setup was employed to perform the analysis at room temperature using a Nicolet smart iTR with a diamond coated ZnSe crystal. Atmospheric contributions were corrected prior to the measurements via measuring and subtracting the background signal.

2.3.3. Thermogravimetric Analysis (TGA)

A Q500 TGA (TA Instruments) was used to assess thermal degradation of the polymer, as well as to verify the presence of any remaining solvent into the sample. The material was heated at a rate of 10 K min^{-1} up to 450 ˚C under air atmosphere.

2.3.4. Differential Scanning Calorimetry (DSC)

The thermochemical behavior of the materials was analyzed using a Q2000 DSC (TA Instruments), equipped with a Refrigerated Cooling System (RCS). The DSC cell is purged with nitrogen gas.

Heating-cooling cycles were performed from -90 ˚C to 140 ˚C at a rate of 10 K min^{-1}, to assess the thermal reversibility of the Diels-Alder adducts. After the first heating cycle, the material stayed isothermal at 140 ˚C to almost completely dissociate into the monomers. These temperatures were chosen to prevent possible side reactions that can give rise to undesired variations in endothermic signals, due to Michael addition or homopolymerization of bismaleimides.

2.3.5. Dynamic Rheometry

Rheological experiments were performed on an AR-G2 stress-controlled rheometer (TA Instruments) equipped with a convection oven as a heating system using air atmosphere and steel parallel plate geometry of 25 mm diameter. Contact pressure was set as 1 N to ensure good contact between the material and the oscillatory plate.

A thermal sweep was performed ranging from 70 ˚C to 130 ˚C at a heating rate of 2 K min^{-1}. During the thermal scan, five different discrete oscillation frequencies following a logarithmic distribution were switched between 0.01 and 1 Hz. A strain of 0.5 % was used and previously proved that is in the linear viscoelastic region.

2.3.6. Dynamic Mechanical Analysis (DMA)

Tensile measurements of the different materials were carried out at room temperature using a Q800 DMA (TA Instruments device) performing stress-strain tests until fracture in controlled strain mode. Rectangular specimens of 7.79 ± 0.44, 5.55 ± 0.03, 0.65 ± 0.18 (mm) were subjected to tensile stresses with a rate of 60 % min^{-1}. The results were determined from the average values of at least ten replicates for each sample.

3. Results and Discussion

3.1. Synthesis and Chemical Characterization

First, the synthesis of the furan-functionalized monomer F5000 was carried out via an irreversible epoxy-amine reaction. Completion of the reaction was evaluated by thermogravimetric analysis concluding that, under the above-mentioned reaction conditions, total conversion was obtained (see Supplementary Information, Figure S2.1).

The furan-functionalized Jeffamine F5000 was reacted with the bismaleimide DPBM to form the Diels-Alder crosslinks of the reversible covalent network, following the scheme available at the Supplementary Information (Figure S1). A stoichiometric ratio r ($r = n_{Maleimide}/n_{Furan}$) of 0.5 is used for the materials studied in this work. The aim is to obtain a low crosslink density in the polymeric network. It was hypothesized that a flexible elastomeric network would be required to manifest a response caused by the external magnetic force without the need to raise the temperature up to too high values, where the material would start to degel or to initiate irreversible side reactions. Hence, the healing experiments can be performed at low enough temperatures to ensure proper mechanochemical stability. Robotics researchers have demonstrated the use of changing the stoichiometric ratio for self-healing materials to (i) alter the thermomechanical properties, (ii) to influence the self-healing behaviour and (iii) to demonstrate successful healing of multi-material soft robotic actuators [43,44].

As described in Section 2.2, once the monomers were fully dissolved, the Fe_3O_4 nanoparticles (NPs) were added to the solution. Mixing under mechanical shaking with an oscillation frequency of 120 rpm in a closed vial environment, so $CHCl_3$ cannot volatilize, was performed to disperse the particles for one day. Different loadings of Fe_3O_4 NPs were employed for the synthesis of different composite compositions to assess the effect on both the magnetic response and the thermomechanical properties of the resulting composites. Table 1 shows the different synthesized composites, numbered as the mass percentage of Fe_3O_4 employed, as well as the bulk material without NPs.

Table 1. Weight and volume fractions of Fe_3O_4 filler in the composites and residual weight of the inorganic filler after thermal degradation of the composite in TGA.

Composite	**Weight fraction (wt% Fe_3O_4)**	**Volume Fraction (vol% Fe_3O_4)**	**Residual weight (m% TGA)**
DPBM-F5000 0.5	0	0	0
MagSH5000 5%	5	1	5,4
MagSH5000 10%	10	2	10,3
MagSH5000 20%	20	5	14,8
MagSH5000 30%	30	8	25,4
MagSH5000 50%	50	17	50,2

With the aim of creating flat films for mechanical testing, the polymerization was carried out onto a Teflon Petri dish, obtaining thin films of around 0.7 mm thickness. The samples were removed from the Petri dish and dried under vacuum at 60 ˚C for two days to eliminate remaining traces of chloroform trapped in the sample. Low vacuum was needed in this case in order to avoid the formation of gas bubbles in the films.

SEM images in Figure 2 show the surface of the different composite films and the bulk polymer, and present how Fe_3O_4 particles are distributed along the matrix. Increasing the amount of Fe_3O_4 results in a higher agglomeration of particles in the final composite, reaching sizes close to 40 μm for the MagSH5000 50% material. The presence of Fe_3O_4 also intensifies the number of surface defects, showing a “river-like pattern” microstructure, achieving the highest defects density for 30 wt% of Fe_3O_4 incorporated. Nevertheless, the density of the defects for MagSH5000 50% appeared to be lower, indicating that Fe_3O_4 particles may prevent the formation of a brittle fracture since the load is transferred from the weaker matrix to the stronger Fe_3O_4. Similar behavior of Fe_3O_4 particles has been previously observed [45].

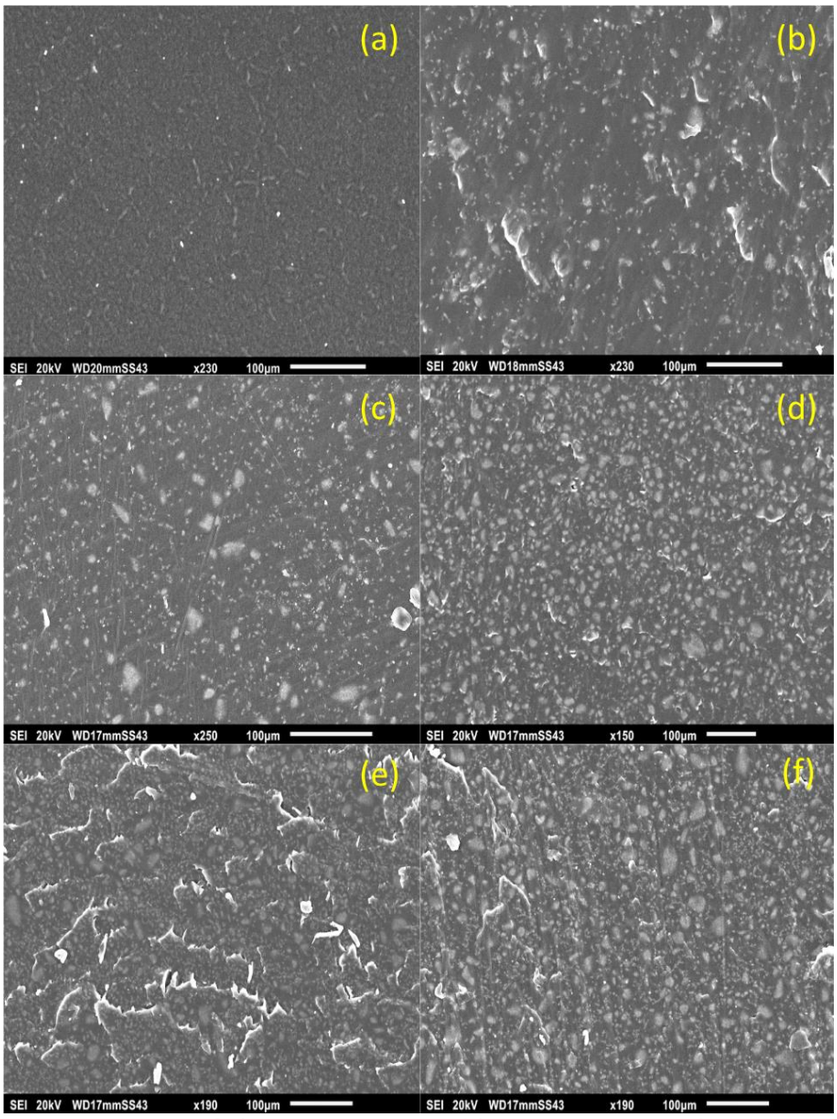

Figure 2: SEM images of a) DPBM-F5000 0.5 b) MagSH5000 5% c) MagSH5000 10% d) MagSH5000 20% e) MagSH5000 30% f) MagSH5000 50%

FT-IR measurements confirm the consumption of the furan and maleimide groups to form the DA adducts. Figure 3 shows the spectra for the furan-functionalized Jeffamine F5000, the bismaleimide DPBM and the final material after reaction with the bismaleimide (DPBM-F5000 0.5). Previous reports couple the stretching mode corresponding to the C=C bond associated with the DA adduct with the signal at 1510 cm^{-1} [21]. However, the presence also at 1514 cm^{-1} previously reported for DPBM of C–C stretching in phenyl groups makes this affirmation unreliable. On the other hand, a small absorption is detected at 1777 cm^{-1}, a common signal attributed to the existence of DA adducts based on furan and maleimide reactions that indicates the formation of DA adducts. Though, due to the presence of large aliphatic C–O absorption generated by PEO structures present in the Jeffamine, the characteristic C–N–C stretch of DA adducts at around 1146 cm^{-1} is hard to assess [46,47]. Looking at the results, it cannot unambiguously ascertain the formation of DA adducts, despite seeing the presence of some distinctive signals because of their formation. However, based on previous studies carried out by the FYSC group, the reactivity between furan and maleimide groups under the proposed conditions is feasible [48]. Additionally, no changes in the chemical composition of the final composite was found looking at the results caused by the inclusion of Fe_3O_4 material, confirming that the magnetic particles did not alter the chemistry of the final polymer in comparison with the bulk counterpart (See Supplementary Information, Figures S3.1 – S3.6).

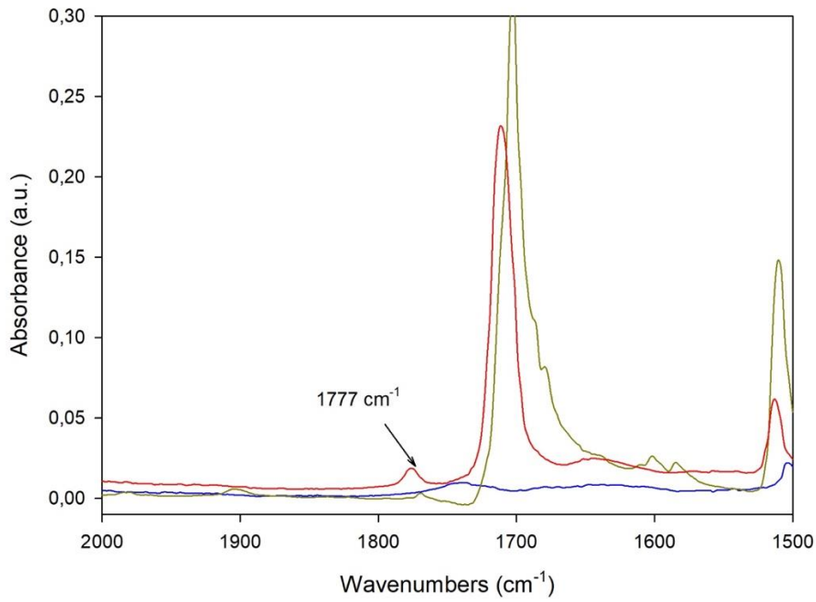

Figure 3. FT-IR spectra of pure DPBM (dark yellow line), pure F5000 (blue line) and DPBM-F5000 0.5 polymer (red line)

3.2. Thermomechanical Analysis of DA composites:

TGA measurements show that the materials are thermally stable up to about 320 ˚C. TGA curves of the bulk polymer and the magnetic composites are available at the Supplementary Information (Figure S2.2). At these temperatures, the polymer network dissociates into the monomers which degrade, and volatile compounds escape from the material, reducing sample weight. Note, however, that these degradation temperatures should not be considered as the maximum temperature for applications or processing of the material, since at temperatures higher than 120–130 ˚C irreversible side reactions can take place, modifying the reversible properties of the DA polymers.

Furthermore, the remaining weight of the samples after degradation of the organic polymer network at temperature up to 400 ˚C relates to the amount of inorganic filler present in the studied composite. It is possible to determine the fraction of NPs dispersed within the analyzed sample y_{NP} from the weight fraction of the composite left after thermal degradation of the organic polymer matrix $y_{composite}$ and taking into account the remaining fraction of the pure polymer matrix y_{matrix} after degradation (green curve in Figure S2.2):

$$y_{\mathrm{NP}} = \frac{y_{\,\mathrm{composite}} - y_{\mathrm{matrix}}}{(1 - y_{\mathrm{matrix}})}$$

It is assumed that no degradation of the inorganic filler occurs, and that the inorganic filler does not affect the rate and extent of degradation of the organic polymer matrix. At low and high filler loadings, the calculated weight fractions (Table 1) match the values used during synthesis, while for 20 and 30 wt% the calculated values deviate, suggesting inhomogeneity in the dispersion of NPs along the polymeric film at these concentrations. In literature, a mass gain in the region of 200 ˚C has been reported for the calcination of pure Fe_3O_4, associated with the oxidation of magnetite to iron (III) oxide in the presence of oxygen [49]. However, this increase was not observed for the current composites, confirming that the Fe_3O_4 particles are protected by the polymeric matrix and preserve their stability.

DSC measurements were performed to evaluate the thermoreversibility of the DA polymeric network. In calorimetry, when heating up the DA polymer networks, two broad endothermic peaks are observed for the cycloreversion of the DA adduct [50]. The first endothermic peak is attributed to the dissociation of the *endo* isomer, which is kinetically more favorable at low temperatures due to secondary interactions between the bulkier

sides resulting in a lower activation energy barrier. The second peak originates from the thermal dissociation of the thermodynamically more stable *exo* isomer.

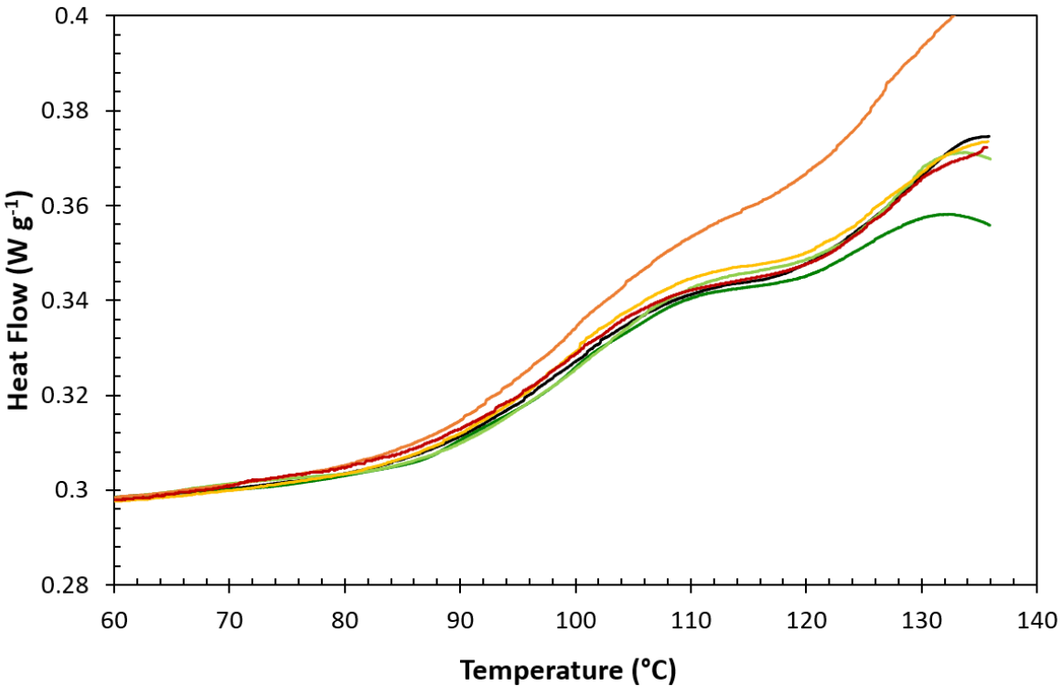

Figure 4. Overlay of DSC thermograms of the different studied systems (DPBM-F5000 0.5: Black; MagSH5000 5%: Dark green; MagSH5000 10%: Green; MagSH5000 20%: Yellow; MagSH5000 30%: Orange; MagSH5000 50%: Red). Heating rate employed is 10 K min^{-1}

The reactivity of the Diels-Alder reaction can be studied using calorimetry, as elaborated by Cuvellier et al. [50]. Figure 4 compares the DSC results of all studied composites with the result for the pure polymer matrix. The experimental heat flow signal from DSC was recalculated to the weight of the polymer matrix only to allow straight forward comparison for all material compositions. The second heating is shown, after a first dissociation cycle to 140 ˚C to eliminate the different thermal histories of the materials. Between the first heating and the second heating the material samples have received the same thermal treatment to allow reliable comparison of the amount of adduct formed during cooling. Fe_3O_4 is a well-known Lewis acid, widely employed in catalysis. In the case of Diels-Alder reaction Lewis acids catalyze the formation of the *endo* adduct over *exo* [51]. From the results in Figure 4, it can be concluded that there is no change in reactivity due to different loadings of Fe_3O_4, as the thermograms overlap and exhibit the same proportions of endo and *exo* adducts. Only for the 30 wt% composite the heat flow signal deviates from the materials with different compositions. This can be explained by the uncertainty of the filler loading due to inhomogeneity of the sample. An overestimation of the filler content leads to a wrong correction of the heat flow signal with respect to the underestimated polymer fraction. This explains why the heat flow signals are larger, while the ratio of the endothermic peaks from the endo and *exo* adducts is the same as for the other materials.

The effect of the filler and the filler loading on the viscoelastic properties is studied using dynamic rheometry. The viscoelastic properties of the composites play an important role in the handling and processing of the networks, and dynamic rheological tests are suitable to study them. Figure 5 compares the phase angle δ of the pure polymer matrix (dark yellow) with the phase angle of the composites at different discrete frequencies during the heating in a dynamic oscillatory measurement. At low temperatures, the phase angle δ is almost equal to 0˚, corresponding to an elastic response. As the temperature increases, gradually more reversible DA bonds are broken and the crosslink density of the network decreases. At a certain point, the phase δ angle starts to increase, as a critical number of bonds is broken. Finally, the phase angle δ nears 90˚, corresponding to a viscous response [52]. At a phase angle of about 60°, the lines at different frequencies cross. The point where the phase angle becomes independent of frequency is referred to as the gel point [53]. At this point, the material goes from a predominantly solid-like behaviour to a predominantly liquid-like

behaviour, and vice versa upon cooling. The temperature for which the critical gel conversion x_{gel} is reached is referred to as the gel transition temperature (T_{gel}). For DPBM-F5000 0.5 the equilibrium T_{gel} equals 104 °C.

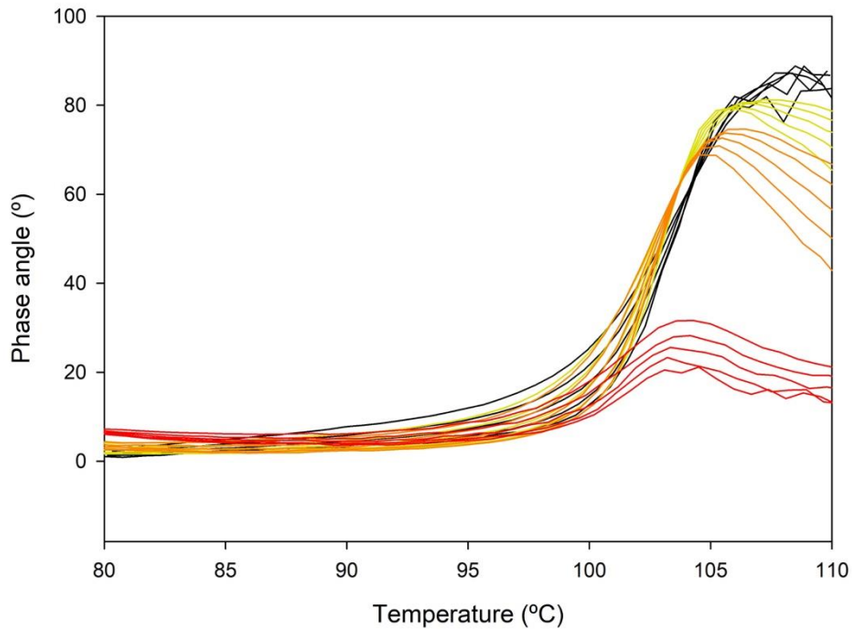

Figure 5. Phase angle (δ) of DPBM-F5000 0.5 (black), MagSH5000 20% (yellow), MagSH5000 30% (orange) and MagSH5000 50% (red) at five discrete frequencies (0.312599 Hz; 0.562301 Hz; 1 Hz; 1.778 Hz; 3,12599 Hz) at 1 K min^{-1}. The phase angles of MagSH5000 5 and 10% are similar to those of DPBM-F5000 0.5 and not shown for clarity.

Table 2. Gel transition temperature, Young's Modulus, fracture strain and stress for the pure polymer network and the magnetic composites.

Composite	**T_{gel} (˚C)**	**E (MPa)**	**$\varepsilon_{fracture}$ (%)**	**$\sigma_{fracture}$ (MPa)**
DPBM-F5000 0.5	104.2	1.12 ± 0.05	191 ± 24	0.62 ± 0.13
MagSH5000 5%	104.5	1.05 ± 0.04	165 ± 21	0.58 ± 0.03
MagSH5000 10%	104.2	1.05 ± 0.06	155 ± 14	0.59 ± 0.01
MagSH5000 20%	103.6	1.24 ± 0.06	139 ± 15	0.67 ± 0.09
MagSH5000 30%	103.8	2.14 ± 1.53	111 ± 46	0,72 ± 0.13
MagSH5000 50%	n.a.	12.14 ± 1.21	53 ± 10	1,29 ± 0.2

The viscoelastic behaviour of the magnetic composites with 5 and 10 wt% NP's was similar to that of the pure polymer matrix due to the limited effect of the small amounts of NP's. Both gel points are also around 104 °C (Table 2). Figure 5 also shows the viscoelastic behaviour of the composites with higher filler loadings. For these composites, the phase angle δ also increases as the material is heated, however, the phase angle does no longer go towards 90° due to the filler-filer interactions. Instead, it goes through a maximum. For the 20 and 30 wt% NP composites, a gel transition temperature T_{gel} could still be determined, as the frequency-independent cross-over was still observed at around the same temperature as for the other materials. The 50 wt% composite does no longer show liquid-like behaviour under the measuring conditions for the small angle oscillatory measurements, as the forces applied on the sample and the amplitude of the oscillation are no longer high enough to make the liquid composite flow due to the increased particle interactions. Still, a clear increase in the phase angle can be observed around the same temperature as for the other materials. Hence, it can be concluded that despite the clear effect of the filler and filler loading on the viscoelastic behaviour of the composites, the gel transition temperature T_{gel} of the polymeric matrix remains the same for all composites. This is supported by the earlier conclusion that the reaction kinetics and thermodynamics of the Diels-Alder reaction remain unchanged in the presence of the Fe_3O_4 NP (DSC, Figure 4). In a control experiment using non-magnetic Al_2O_3 nanoparticles similar results were obtained, not showing any influence on the reactivity of the reversible Diels-Alder reaction (Figure S5).

To evaluate the mechanical properties of the solid composites, tensile tests were performed until failure of the material. Full plots of the DMA tensile experiments are available in the Supplementary Information (Figure S4). The values for the Young's moduli and fracture strains are compared in Figure 6 for all composites. The Young's Modulus E, calculated as the slope in the linear region of the curves at strain values from 0 to 5 %, slightly increased with the filler content, abruptly increasing for the 50 wt% composite. The same abrupt change can be seen for the fracture stress. Conversely, the fracture strain decreases gradually with increasing filler content, almost linearly with the filler content (Figure 6). MagSH5000 30% exhibits a different mechanical behavior depending of in which zone of the composite film is the specimen chopped (see cyan curves in Figure S4). This is explained by inhomogeneities in the distribution of Fe_3O_4 particles along the polymeric matrix. Young's Modulus of MagSH5000 30% was determined as the mean value of different specimens taken from different parts of the composite film, resulting in a large error on the calculated properties.

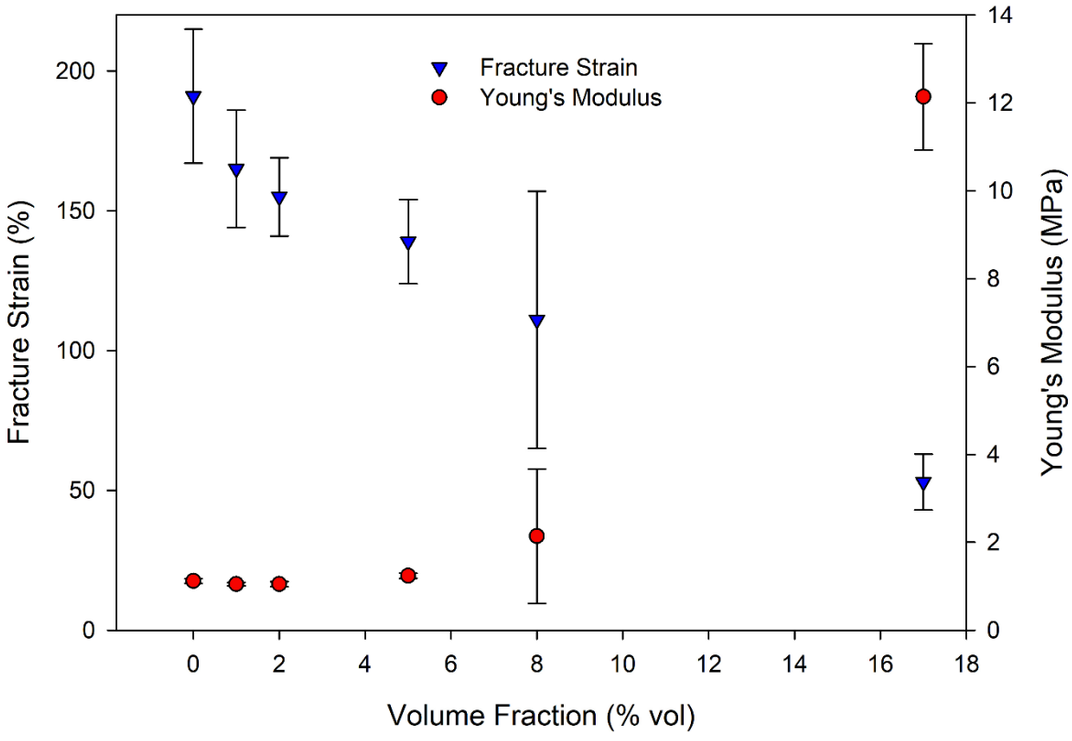

Figure 6. Fracture strain (blue triangles) and Young's Modulus (red circles) values as a function of the volume fraction of the different composites

3.3. Magnetic and Conventional Healing Experiments

A setup was prepared for the healing experiments using a magnetic driving force, as shown schematically in Figure 7. Samples (1) were clamped (3) inside an oven underneath a conventional ring magnet (2), with the broken gap aligned alongside the magnet (roughly 2-3 mm of separation). The temperature of the oven was monitored using a thermocouple (4) next to the sample. A piece of the sample was sliced off using a scalpel. Length and width of scissions were 4.67 ± 1.13 and 2.42 ± 0.66 (mm), respectively, for the different experiments. Specimens with thicknesses of 2-3 mm were tested. Note that the size of the damage is comparable to the thickness of the samples.

The optical photographs in Figure 7 show the behavior of different composites when heated up to a temperature where the mobility of the network was high enough to be influenced by the external magnetic force and to align the damage with the magnet, closing the fracture. Temperatures were optimized for each sample and are shown in Table 3 by heating the broken materials next to the magnet (as indicated in Figure 7) at different temperatures and studying the response of the material after 1 h of experiment, which was

chosen as the time limit for the healing process. The chosen temperature was the lowest at which the material was able to close the damage within the proposed times. Samples without Fe_3O_4 did not show any change after one hour of experiment at temperatures ranging from 95-97 ˚C, where the material is still below the gel point. Healing experiments were carried out at least four times to check reproducibility of the experiments.

Figure 7. The top scheme gives a schematic representation of the setup built inside the annealing oven: (1) composite sample, (2) magnet, (3) clamp (4) thermocouple. The

circular magnet (poles shown) was mounted such that the field lines would travel from left to right through the sample. An example of the direction of the magnetic field lines is shown. Photographs show the healing experiments of MagSH5000 5% a) before healing and b) after healing, MagSH5000 10% c) before healing and d) after healing, and MagSH5000 20% e) before healing and f) after healing.

The temperatures required to fully close the damage of the MagSH5000 5% composite (Figure 7a and 7b) were too, as can be observed by the droplet coming off of the sample and the material that has moved towards the magnet. The temperatures of around 99 ˚C to close the damage after 30 – 60 minutes of experiment are too close to the gel point temperature of 104 ˚C. At these temperatures the dynamic reversibility of the DA reaction becomes so fast that the material managed to flow under the application of the magnetic force. MagSH5000 10% (Figure 7c and 7d) healed the gap at a lower temperature than the 5 wt% composite (96-97˚C) after one hour of experiment while retaining the solid-like state. If the sample was clamped too tight, permanent creep at the bottom may still take place generated by the pressure of the clamp at the elevated temperatures and the fixed geometry of the clamp during cooling down the material. However, the damage was recovered in a very good fashion under these environmental conditions. MagSH5000 20% (Figure 7e and 7f) closed the gap after 20 min in the oven at a temperature of 92˚C, and the sample remained in good conditions after cooling down. The damage surfaces were properly aligned, the gap successfully closed, and there were no signs of deformation caused by clamping at this temperature.

Lack of reproducibility was seen for MagSH5000 30%, exhibiting distinct behaviours in different measurements, due to the inhomogeneity of the distribution of Fe_3O_4 particles along the matrix. Thus, the MagSH5000 30% is not considered reliable for the magnetically induced healing evaluation. For MagSH5000 50%, temperatures much lower could be used to close the damage, however, the healing of the gap once the material was cooled down was too poor. Hence, MagSH5000 30% and MagSH5000 50% materials were rejected for further healing characterization.

A control experiment was performed using non-magnetic Al_2O_3 nanoparticles as a filler to assess the effect of the filler on the healing properties (Figure S6). Similarly to the unfilled material, no closing of the damage was observed. The experiment serves to demonstrate that the damage closure is indeed due to the presence of a magnetic interaction between the magnetic composites and the magnet.

Based on the obtained results, MagSH5000 10% and MagSH5000 20% exhibited the best mechanical response using less Fe_3O_4 NP's as well as good thermomechanical properties compared with the rest of the composites. After healing, no relevant deformations were found on MagSH5000 20% caused by clamping. In the case of MagSH5000 10%, controlling the experimental timing it makes possible to diminish substantially clamping influence and stress-strain curves demonstrate that elastomeric properties are similar to that of their analogues with lower loadings of Fe_3O_4 (see Table 2).

Table 3. Healing temperatures (1 h) and resulting healing efficiencies for gap closure under magnetic activation

Composite	**Healing Temperatures (˚C)**	**Healing Efficiency (%)**
DPBM-F5000 0.5	n.a.	103
MagSH5000 5%	99-100	100*
MagSH5000 10%	96-97	85
MagSH5000 20%	91-92	56
MagSH5000 30%	88-93	Not determined˚
MagSH5000 50%	86-87	Not determined˚

* The damage gap closed successfully, however the sample did not retain its shape

˚ Lack of reproducibility caused by inhomogeneities in case of MagSH5000 30% material and poor healing observed during healing experiments for MagSH5000 50%

Quantitative evaluation of the healing efficiency of the final pieces, presented in Figure 7 is not possible since the deformation of the material after filling the empty gap avoid it, so the possibility to obtain a homogeneously shaped specimen for a stress-strain test was not possible. Conventional stress-strain tensile tests until fracture were performed for the pure polymer matrix and the 5, 10 and 20 wt% composites using rectangular specimens of the same dimensions as for the tensile measurements in Figure 6. The samples were healed at 92 ˚C (temperature used for MagSH5000 20% magnetic healing experiments) for one hour, cooled down at 0,5 K min^{-1} and left at room temperature for three days to restore the equilibrium conditions, and finally submitted to the same tensile test to evaluate the mechanical properties after healing. MagSH5000 30% and MagSH5000 50% were not considered for this purpose due to the lack of their reproducibility and bad mechanical response.

Healing efficiency (η) was considered as the ratio between the fracture stress after healing and before healing:

$$\eta = \frac{\sigma_a}{\sigma_b}$$

Healing efficiency data is compilated in Table 3. Fracture stress and Young's Modulus before and after healing of the proposed materials are presented in Figure 8. Although these results are not applicable for the healing experiments using a magnet due to the different conditions evaluated and different morphologies, they may be employed as a comparison of the different materials in terms of the efficiency of their healing properties. A total recovery of the mechanical strength was observed for DPBM-F5000 0.5 and MagSH5000 5% by evaluating the tensile properties. For MagSH5000 10% and MagSH5000 20%, a lower recovery of the mechanical properties was observed, and failure occurred at lower strain values at the same location as where the cuts were previously made. The assumption of this deterioration of the tensile properties is that Fe_3O_4 aggregates are too big, so the mobility of furan and maleimide groups along the broken gap is limited. The size of some of the particles found in SEM results is close to the film thickness of the composite. However, the fracture stress value recovered for MagSH5000 10% is perfectly acceptable, achieving a healing efficiency of the process of 85% allowing the material to be reused in a wide range of applications in the same way as the original material was employed. MagSH5000 20% exhibited a lower recovery but a much faster closure of the broken gap, being applicable on duties where low stress or strains are required.

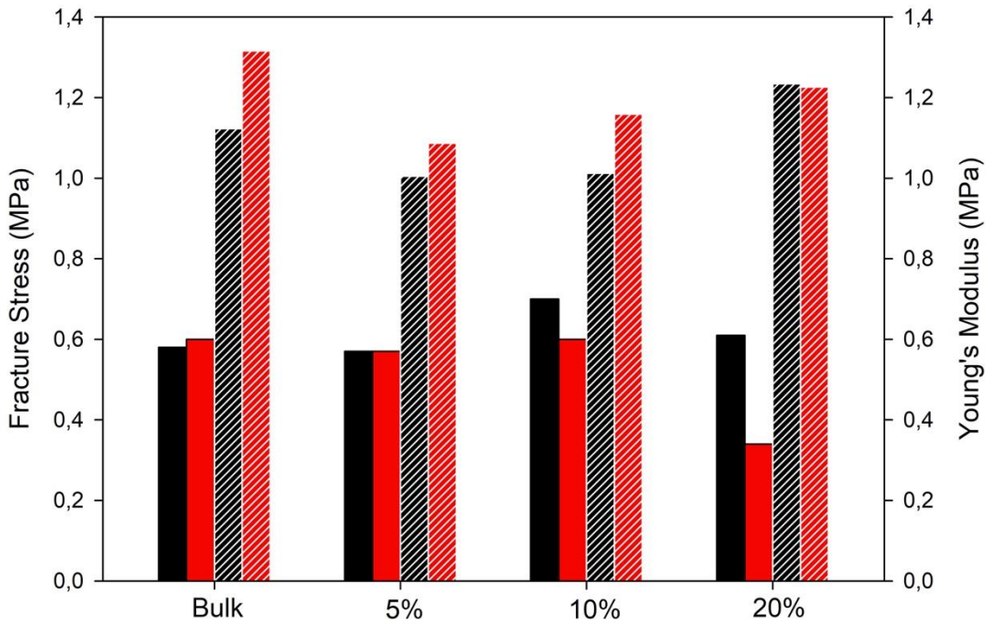

Figure 8. Fracture stress (solid) and Young's Modulus (dashed) for bulk DPBM-F5000 0.5 and MagSH5000 20% before (black) and after (red) healing at 92˚C for 1 hour

While not all of the mechanical properties of the material were fully recovered for MagSH5000 10% and MagSH5000 20%, the idea of using magnetic particles to enhance the healing performance of self-healing materials remains as a promising and challenging alternative, and this first proof of concept opens a door for the preparation of a wide range of different composites with different healing methods and different magnetic materials, and the optimization of dispersion and particle size may lead to a material with same mechanochemical properties as the bulk polymeric counterpart but with the advantage of being magnetically healable.

Conclusions:

A novel approach has been developed in this study with the aim of improving the healing of large damage in self-healing materials by using a magnetic field as the driving force to close large damage sizes and to improve the contact between the broken surfaces. Magnetic Fe_3O_4 nanoparticles were incorporated in an elastomeric polymer network with reversible Diels-Alder crosslinks to create self-healing magnetic elastomeric composites. Healing experiments were performed by placing a magnet next to a large damage and increasing the environmental temperature. The increased mobility at elevated temperatures allowed for successful closing of the damage area.

Composites with different filler contents were studied to optimize the magnetic response of the material with respect to the healing behaviour. Promising results were obtained for composites with 10 and 20 wt% of magnetic nanoparticles, as the mechanical properties were similar to those of the bulk material in a considerable range of strains and stresses (Young's modulus values of 1.07 and 1.27 MPa for the composites with a Fe_3O_4 loading of 10% and 20%, respectively, compared to 1.12 MPa of the bulk material) and exhibited a good magnetic response. For the mentioned composites, sufficient mobility and successful closing of the damage could be achieved at temperatures where the material could retain its structural integrity, without the need to increase the temperature too high so the material would start to degel. Healing efficiencies of 85 % and 56 % were obtained for the 10 wt% and 20 wt% composites, respectively.

Lower filler contents resulted in higher healing efficiencies around 100 %. However, the temperature needed to be raised too high to obtain a noticeable magnetic response, which resulted in viscous flow for the 5 wt% composite under the magnetic force. At the other extreme, the 30 and 50 wt% composites demonstrated excellent magnetic response and closing of the damage, while the healing efficiency dramatically suffered from the limited chain mobility due to the high filler loadings.

While the feasibility study was successful and a clear optimum in composite composition could be found, the performance of the magnetic composites can still significantly be improved by (i) changing the flexibility and mobility of the polymer matrix and the thermomechanical behaviour, (ii) changing the nanoparticle size and dispersion quality of the Fe_3O_4 particles to reach better magnetic properties at lower particle loadings, reducing the adverse effects on the viscoelastic behaviour and healing efficiency and (iii) evaluating other metallic nanoparticles that may exhibit stronger magnetic properties at lower loadings. Fe_3O_4 is stated as a promising, cheap and non-toxic alternative for the synthesis of magnetic composites. Considering the ability to close and heal large damage, while preserving good mechanical properties and structural integrity these self-healing magnetic composites are very interesting candidates for applications in soft robotics.

Declaration of competing interest:

The authors declare no competing interests.

CRediT authorship contribution statement:

Kenneth Cerdan: Conceptualization, Investigation, Writing – original draft. **Guy Van Assche:** Supervision, Resources. **Peter Van Puyvelde:** Supervision, Writing – review & editing. **Joost Brancart:** Conceptualization, Supervision, Data curation, Writing – review & editing

Acknowledgements:
The authors thank the Research Foundation Flanders (FWO-Vlaanderen) for financial support for the FWO SBO project AMSeR (G028218N) and the postdoctoral fellowship of Joost Brancart (12W4719N).

Bibliography:

[1] M. Wei, Y. Gao, X. Li, M.J. Serpe, Stimuli-responsive polymers and their applications, Polym. Chem. (2017). https://doi.org/10.1039/c6py01585a.
[2] M.A.C. Stuart, W.T.S. Huck, J. Genzer, M. Müller, C. Ober, M. Stamm, G.B. Sukhorukov, I. Szleifer, V. V. Tsukruk, M. Urban, F. Winnik, S. Zauscher, I. Luzinov, S. Minko, Emerging applications of stimuli-responsive polymer materials, Nat. Mater. (2010). https://doi.org/10.1038/nmat2614.
[3] A.A. Nazeer, M. Madkour, Potential use of smart coatings for corrosion protection of metals and alloys: A review, J. Mol. Liq. (2018). https://doi.org/10.1016/j.molliq.2018.01.027.
[4] J. Brancart, R. Verhelle, J. Mangialetto, G. Van Assche, Coupling the Microscopic Healing Behaviour of Coatings to the Thermoreversible Diels-Alder Network Formation, Coatings. (2018). https://doi.org/10.3390/coatings9010013.
[5] J.M. Knipe, N.A. Peppas, Multi-responsive hydrogels for drug delivery and tissue engineering applications, Regen. Biomater. (2014). https://doi.org/10.1093/rb/rbu006.
[6] R. Parilti, J. Caprasse, R. Riva, M. Alexandre, H. Vandegaart, C. Bebrone, C. Dupont-Gillain, S.M. Howdle, C. Jérôme, Antimicrobial peptide encapsulation and sustained release from polymer network particles prepared in supercritical carbon dioxide, J. Colloid Interface Sci. (2018). https://doi.org/10.1016/j.jcis.2018.07.125.
[7] N.A. Nguyen, K.M. Meek, C.C. Bowland, S.H. Barnes, A.K. Naskar, An Acrylonitrile-Butadiene-Lignin Renewable Skin with Programmable and Switchable Electrical Conductivity for Stress/Strain-Sensing Applications, Macromolecules. (2018). https://doi.org/10.1021/acs.macromol.7b02336.
[8] Y. Wang, C. Zhu, R. Pfattner, H. Yan, L. Jin, S. Chen, F. Molina-Lopez, F. Lissel, J. Liu, N.I. Rabiah, Z. Chen, J.W. Chung, C. Linder, M.F. Toney, B. Murmann, Z. Bao, A highly stretchable, transparent, and conductive polymer, Sci. Adv. (2017). https://doi.org/10.1126/sciadv.1602076.
[9] S. Terryn, J. Brancart, D. Lefeber, G. Van Assche, B. Vanderborght, Self-healing soft pneumatic robots, Sci. Robot. (2017). https://doi.org/10.1126/scirobotics.aan4268.
[10] W. Hu, G.Z. Lum, M. Mastrangeli, M. Sitti, Small-scale soft-bodied robot with multimodal locomotion, Nature. (2018). https://doi.org/10.1038/nature25443.
[11] M. Samadzadeh, S.H. Boura, M. Peikari, S.M. Kasiriha, A. Ashrafi, A review on self-healing coatings based on micro/nanocapsules, Prog. Org. Coatings. (2010). https://doi.org/10.1016/j.porgcoat.2010.01.006.
[12] A. Cuvellier, A. Torre-Muruzabal, G. Van Assche, K. De Clerck, H. Rahier, Selection of healing agents for a vascular self-healing application, Polym. Test. (2017). https://doi.org/10.1016/j.polymertesting.2017.07.013.
[13] F. Herbst, D. Döhler, P. Michael, W.H. Binder, Self-healing polymers via supramolecular forces, Macromol. Rapid Commun. (2013). https://doi.org/10.1002/marc.201200675.
[14] R.J. Wojtecki, M.A. Meador, S.J. Rowan, Using the dynamic bond to access macroscopically responsive structurally dynamic polymers, Nat. Mater. (2011). https://doi.org/10.1038/nmat2891.
[15] Y. Zhang, A.A. Broekhuis, F. Picchioni, Thermally self-healing polymeric materials: The next step to recycling thermoset polymers?, Macromolecules. (2009). https://doi.org/10.1021/ma8027672.
[16] C. García-Astrain, A. Gandini, C. Peña, I. Algar, A. Eceiza, M. Corcuera, N. Gabilondo, Diels-Alder “click” chemistry for the cross-linking of furfuryl-gelatin-polyetheramine

hydrogels, RSC Adv. (2014). https://doi.org/10.1039/c4ra06122e.
[17] G. Scheltjens, M.M. Diaz, J. Brancart, G. Van Assche, B. Van Mele, A self-healing polymer network based on reversible covalent bonding, in: React. Funct. Polym., 2013. https://doi.org/10.1016/j.reactfunctpolym.2012.06.017.
[18] U. Pindur, G. Lutz, C. Otto, Acceleration and Selectivity Enhancement of Diels-Alder Reactions by Special and Catalytic Methods, Chem. Rev. (1993). https://doi.org/10.1021/cr00018a006.
[19] J. Yli-Kauhaluoma, Diels-Alder reactions on solid supports, Tetrahedron. (2001). https://doi.org/10.1016/S0040-4020(01)00506-3.
[20] M.M. Diaz, G. Van Assche, F.H.J. Maurer, B. Van Mele, Thermophysical characterization of a reversible dynamic polymer network based on kinetics and equilibrium of an amorphous furan-maleimide Diels-Alder cycloaddition, Polymer (Guildf). (2017). https://doi.org/10.1016/j.polymer.2017.05.058.
[21] G. Scheltjens, J. Brancart, I. De Graeve, B. Van Mele, H. Terryn, G. Van Assche, Self-healing property characterization of reversible thermoset coatings, in: J. Therm. Anal. Calorim., 2011. https://doi.org/10.1007/s10973-011-1381-4.
[22] P.A. Pratama, M. Sharifi, A.M. Peterson, G.R. Palmese, Room temperature self-healing thermoset based on the diels-alder reaction, ACS Appl. Mater. Interfaces. (2013). https://doi.org/10.1021/am403459e.
[23] P. Buono, A. Duval, L. Averous, Y. Habibi, Thermally healable and remendable lignin-based materials through Diels – Alder click polymerization, Polymer (Guildf). (2017). https://doi.org/10.1016/j.polymer.2017.11.022.
[24] E.D. Rodriguez, X. Luo, P.T. Mather, Linear/network poly(ε-caprolactone) blends exhibiting shape memory assisted self-healing (SMASH), ACS Appl. Mater. Interfaces. (2011). https://doi.org/10.1021/am101012c.
[25] M.D. Hager, S. Bode, C. Weber, U.S. Schubert, Shape memory polymers: Past, present and future developments, Prog. Polym. Sci. (2015). https://doi.org/10.1016/j.progpolymsci.2015.04.002.
[26] S.R. White, J.S. Moore, N.R. Sottos, B.P. Krull, W.A. Santa Cruz, R.C.R. Gergely, Restoration of large damage volumes in polymers, Science (80-.). (2014). https://doi.org/10.1126/science.1251135.
[27] B. Tudu, A. Tiwari, Recent Developments in Perpendicular Magnetic Anisotropy Thin Films for Data Storage Applications, Vacuum. (2017). https://doi.org/10.1016/j.vacuum.2017.01.031.
[28] M. Dolci, J.F. Bryche, C. Leuvrey, S. Zafeiratos, S. Gree, S. Begin-Colin, G. Barbillon, B.P. Pichon, Robust clicked assembly based on iron oxide nanoparticles for a new type of SPR biosensor, J. Mater. Chem. C. (2018). https://doi.org/10.1039/c8tc01166d.
[29] R.A. Meyer, J.J. Green, Biodegradable polymer iron oxide nanocomposites: The future of biocompatible magnetism, Nanomedicine. (2015). https://doi.org/10.2217/nnm.15.165.
[30] H.L. Fan, S.F. Zhou, W.Z. Jiao, G.S. Qi, Y.Z. Liu, Removal of heavy metal ions by magnetic chitosan nanoparticles prepared continuously via high-gravity reactive precipitation method, Carbohydr. Polym. (2017). https://doi.org/10.1016/j.carbpol.2017.07.050.
[31] Y. Wang, L. Ding, C. Zhao, S. Wang, S. Xuan, H. Jiang, X. Gong, A novel magnetorheological shear-stiffening elastomer with self-healing ability, Compos. Sci. Technol. (2018). https://doi.org/10.1016/j.compscitech.2018.10.019.
[32] M. Ojeda, A. Pineda, A.A. Romero, V. Barrõn, R. Luque, Mechanochemical synthesis of maghemite/silica nanocomposites: Advanced materials for aqueous room-temperature catalysis, ChemSusChem. (2014). https://doi.org/10.1002/cssc.201400055.
[33] M.D. Marquez-Medina, P. Prinsen, H. Li, K. Shih, A.A. Romero, R. Luque, Continuous-Flow Synthesis of Supported Magnetic Iron Oxide Nanoparticles for Efficient Isoeugenol Conversion into Vanillin, ChemSusChem. (2018). https://doi.org/10.1002/cssc.201701884.
[34] Y. Zhang, B. Yang, X. Zhang, L. Xu, L. Tao, S. Li, Y. Wei, A magnetic self-healing hydrogel, Chem. Commun. (2012). https://doi.org/10.1039/c2cc34745h.
[35] W. Xie, Q. Gao, Z. Guo, D. Wang, F. Gao, X. Wang, Y. Wei, L. Zhao, Injectable and

self-healing thermosensitive magnetic hydrogel for asynchronous control release of doxorubicin and docetaxel to treat triple-negative breast cancer, ACS Appl. Mater. Interfaces. (2017). https://doi.org/10.1021/acsami.7b10699.
[36] B.J. Adzima, C.J. Kloxin, C.N. Bowman, Externally triggered healing of a thermoreversible covalent network via self-limited hysteresis heating, Adv. Mater. (2010). https://doi.org/10.1002/adma.200904138.
[37] N. Hohlbein, A. Shaaban, A.M. Schmidt, Remote-controlled activation of self-healing behavior in magneto-responsive ionomeric composites, Polymer (Guildf). (2015). https://doi.org/10.1016/j.polymer.2015.04.024.
[38] C.C. Corten, M.W. Urban, F. Shelby, Repairing polymers using an oscillating magnetic field, Adv. Mater. (2009). https://doi.org/10.1002/adma.200901940.
[39] S. Schäfer, G. Kickelbick, Diels-Alder Reactions on Surface-Modified Magnetite/Maghemite Nanoparticles: Application in Self-Healing Nanocomposites, ACS Appl. Nano Mater. (2018). https://doi.org/10.1021/acsanm.8b00308.
[40] X.Q. Feng, G.Z. Zhang, Q.M. Bai, H.Y. Jiang, B. Xu, H.J. Li, High Strength Self-Healing Magnetic Elastomers with Shape Memory Effect, Macromol. Mater. Eng. (2016). https://doi.org/10.1002/mame.201500226.
[41] A.J. Bandodkar, C.S. López, A.M.V. Mohan, L. Yin, R. Kumar, J. Wang, All-printed magnetically self-healing electrochemical devices, Sci. Adv. (2016). https://doi.org/10.1126/sciadv.1601465.
[42] M.S. Kharasch, F. Kawahara, W. Nudenberg, The mechanism of action of inhibitors in free radical initiated polymerizations at low temperatures, J. Org. Chem. (1954). https://doi.org/10.1021/jo01377a015.
[43] E. Roels, S. Terryn, J. Brancart, G. Van Assche, B. Vanderborght, A multi-material self-healing soft gripper, in: RoboSoft 2019 - 2019 IEEE Int. Conf. Soft Robot., 2019. https://doi.org/10.1109/ROBOSOFT.2019.8722781.
[44] S. Terryn, E. Roels, J. Brancart, G. Van Assche, B. Vanderborght, Self-Healing and High Interfacial Strength in Multi- Material Soft Pneumatic Robots via Reversible Diels –, (2020) 1–17. https://doi.org/10.3390/act9020034.
[45] J. Guo, H. Song, H. Liu, C. Luo, Y. Ren, T. Ding, M.A. Khan, D.P. Young, X. Liu, X. Zhang, J. Kong, Z. Guo, Polypyrrole-interface-functionalized nano-magnetite epoxy nanocomposites as electromagnetic wave absorbers with enhanced flame retardancy, J. Mater. Chem. C. (2017). https://doi.org/10.1039/c7tc01502j.
[46] C. García-Astrain, A. Gandini, D. Coelho, I. Mondragon, A. Retegi, A. Eceiza, M.A. Corcuera, N. Gabilondo, Green chemistry for the synthesis of methacrylate-based hydrogels crosslinked through Diels–Alder reaction, Eur. Polym. J. (2013). https://doi.org/10.1016/j.eurpolymj.2013.09.004.
[47] C. Gaina, O. Ursache, V. Gaina, E. Buruiana, D. Ionita, Investigation on the thermal properties of new thermo-reversible networks based on poly(vinyl furfural) and multifunctional maleimide compounds, Express Polym. Lett. (2012). https://doi.org/10.3144/expresspolymlett.2012.14.
[48] G. Scheltjens, J. Brancart, I. De Graeve, B. Van Mele, H. Terryn, G. Van Assche, Self-healing property characterization of reversible thermoset coatings, in: J. Therm. Anal. Calorim., 2011. https://doi.org/10.1007/s10973-011-1381-4.
[49] C. Meiorin, D. Muraca, K.R. Pirota, M.I. Aranguren, M.A. Mosiewicki, Nanocomposites with superparamagnetic behavior based on a vegetable oil and magnetite nanoparticles, Eur. Polym. J. (2014). https://doi.org/10.1016/j.eurpolymj.2014.01.018.
[50] A. Cuvellier, R. Verhelle, J. Brancart, B. Vanderborght, G. Van Assche, H. Rahier, The influence of stereochemistry on the reactivity of the Diels-Alder cycloaddition and the implications for reversible network polymerization, Polym. Chem. (2019). https://doi.org/10.1039/c8py01216d.
[51] D. Yepes, P. Pérez, P. Jaque, I. Fernández, Effect of Lewis acid bulkiness on the stereoselectivity of Diels-Alder reactions between acyclic dienes and α,β-enals, Org. Chem. Front. (2017). https://doi.org/10.1039/c7qo00154a.
[52] C. Vizireanu, A. Ionescu, D. Istrati, F. Dima, Rheologic behavior of pastry creams, Sci. Study Res. Chem. Chem. Eng. Biotechnol. Food Ind. (2012).
[53] H.H. Winter, Can the gel point of a cross-linking polymer be detected by the G' – G" crossover?, Polym. Eng. Sci. (1987). https://doi.org/10.1002/pen.760272209.